

AMMONIA DECOMPOSITION
ON NiPt SUPPORTED ON γ -ALUMINA:
A STUDY OF STABILITY OF REAL CATALYSTS

by

Jacob Weiner

A thesis submitted to the Faculty of the University of Delaware in partial fulfillment of the requirements for the degree of Master of Chemical Engineering

Spring 2012

© 2012 Jacob Weiner
All Rights Reserved

AMMONIA DECOMPOSITION
ON NiPt SUPPORTED ON γ -ALUMINA:
A STUDY OF STABILITY OF REAL CATALYSTS

by

Jacob Weiner

Approved: _____
Jingguang G. Chen, Ph.D.
Professor in charge of thesis on behalf of the Advisory Committee

Approved: _____
Dionisios G. Vlachos, Ph.D.
Professor in charge of thesis on behalf of the Advisory Committee

Approved: _____
Norman J. Wagner, Ph.D.
Chair of the Chemical Engineering Department

Approved: _____
Babatunde A. Ogunnaike, Ph.D.
Interim Dean of the College of Engineering

Approved: _____
Charles G. Riordan, Ph.D.
Vice Provost for Graduate and Professional Education

ACKNOWLEDGMENTS

I would like to thank my advisers Jingguang Chen and Dionisios Vlachos. I would also like to thank my family and friends for their unending support.

TABLE OF CONTENTS

LIST OF TABLES	v
LIST OF FIGURES	vi
ABSTRACT	vii
Chapter	
1 INTRODUCTION	1
2 METHODS	8
Microkinetic Modeling	8
Synthesis	9
CO Pulse Chemisorption	9
Extended X-ray absorption fine structure (EXAFS)	10
Flow Reactor Studies	12
FTIR Batch studies	12
3 RESULTS	14
Microkinetic Modeling	14
Flow Reactor	14
Batch Reactor	15
Steady-State Flow Reactor	19
Batch Reactor	20
EXAFS	22
4 DISCUSSION	23
5 CONCLUSIONS	25
REFERENCES	27

LIST OF TABLES

Table 2.1	List of Reactions in Ammonia Decomposition Mechanism.....	8
Table 3.2	Summary Table of Rate Constants of Different Metal Catalysts	21
Table 3.3	Summary Chart of EXAFS Results (Coordination Number, Bond Distance, Bond Type) Comparing the Catalyst in a Reducing Environment to the Same Catalyst in Ammonia	22

LIST OF FIGURES

Figure 3.1	Ammonia Conversion Predicted by Model at Laboratory Conditions Compared to Thermodynamic Equilibrium.....	15
Figure 3.2	Model Predicted Ammonia Concentration as a Function of Time	16
Figure 3.3	Coverages of Nitrogen and Hydrogen Found by Model in Batch Reactor.....	17
Figure 3.4	Comparing the Coverages at Low Contact Times for Both Systems	18
Figure 3.5	Steady-State Turnover Frequencies Comparing Different Metal Catalysts	19
Figure 3.6	Comparing Ammonia Concentration as a Function of Time Across Different Metal Catalysts	21

ABSTRACT

Ammonia decomposition is an important reaction due to its impact that it will have on the hydrogen economy. Hydrogen has been found to be a possible source of alternative energy with the application of hydrogen fuel cells. However, the major difficulty with hydrogen, as an alternative energy source, is its low energy density. Hydrogen is a low-density gas, and in order for its use in automobiles to be economically plausible, large tanks under high pressure would have to be employed. The result would limit space available in automobiles for other purposes and pose significant safety issues. As an alternative ammonia has been proposed as a means to store hydrogen chemically, due to its increased energy density. At moderate pressures (~9 atm) ammonia is a liquid, and could be adapted into the current liquid fuel infrastructure. In addition, the decomposition of ammonia would not produce carbon monoxide, a known poison of fuel cell electrodes. Thus, the ammonia decomposition reaction is one piece of the mechanism that could make hydrogen a viable alternative energy source.

The work of Hansgen et al. examined ammonia decomposition through computational studies and surface science experiments on monolayer bimetallic surfaces. The Ni-Pt-Pt(111) configuration of NiPt was found to show favorable results

for ammonia decomposition. In a reducing environment, the subsurface configuration of Pt-Ni-Pt(111) is thermodynamically preferred, and the surface configuration of Ni-Pt-Pt(111) is most stable in an oxidizing environment. The focus of this work is on reactor experiments at ambient pressure with supported catalysts. Experiments performed using supported catalysts will validate predictions made by computations and surface science experiments. The experiments in this work will bridge the pressure and materials gap from surface science experiments to real supported catalysts.

NiPt catalysts were synthesized and characterized by CO chemisorptions and EXAFS. Batch reactor and flow reactor experiments were performed to measure catalytic activity. There were no observations made of increased activity with the bimetallic catalyst. This is evidence of Ni-terminated surface not present in the reactor environment, indicating that the DFT calculations and surface science experiments performed previously within the group do not accurately approximate the real catalyst. Microkinetic modeling was used to find the expected results in the batch reactor and flow reactor. It was predicted that the Ni never segregates to the surface of the catalyst due to the large amount of hydrogen present on the surface of the catalyst and an insignificant amount of nitrogen bound to the surface.

Chapter 1

INTRODUCTION

Solar hydrogen is a reliable source of energy that in the future can be developed for a truly renewable and sustainable global energy economy. Through the application of hydrogen fuel cells, electricity can be produced as hydrogen is consumed, with water as the only byproduct. Water is a much more environmentally friendly byproduct than carbon dioxide, which is currently produced from utilizing fossil fuels. If emitted water is harnessed and collected, it could be used in the future as a potential clean source of water. Also, no longer producing carbon dioxide as a byproduct would stop harming the earth's precious atmosphere. However, there are significant reasons as to why we still continue to rely on fossil fuels.

The major difficulty with utilizing hydrogen as an alternative energy source is energy storage. The application of hydrogen to automobiles is an interesting problem because the energy must be stored onboard the vehicle due to the mobile nature of transportation. For fossil fuels, energy storage is not a problem because at ambient temperatures and pressures gasoline is a liquid. There is already an infrastructure in place for transporting gasoline from the refineries, to the gas pump to the vehicle. On the other hand, hydrogen is a gas at ambient conditions, so the current infrastructure would need to be significantly altered to transport it long distances from the plant to the vehicle. Also hydrogen has a low energy density because it is a low-density gas.

Large bulky tanks under high pressure would have to be employed to use hydrogen in cars directly. These obstacles would limit space available for passengers and cargo and pose significant safety issues because of explosion hazards.

One proposed solution is to produce electricity at a centralized location and simply store it. The current gravimetric and volumetric energy densities of batteries are 0.2 kWhkg^{-1} and 200 kWhm^{-3} , respectively. The average European car uses 8.6L of gasoline every 100 km, which is equivalent to 20 kWh. So in order to drive 500 km, (the range of most cars can on one tank of gas) would require a battery that weighed 500 kg and had a volume of 2.5 m^3 .¹ A battery of that size would add to the weight of the car, and the loss in cargo space necessary for that amount of energy to be stored, would not be economically feasible.

Another proposed mechanism for utilizing solar hydrogen is to store the hydrogen in a chemical energy carrier, and then catalytically produce the hydrogen onboard as it is needed. Ammonia has been proposed as an efficient means to store hydrogen chemically, due to its increased energy density. Ammonia has a greater volumetric energy density than fossil fuels and only a slightly smaller gravimetric energy density. Ammonia as an energy carrier would circumvent the need for bulky or high-pressure tanks, while still having the environmental benefits of utilizing hydrogen.² At moderate pressures (~9 atm) ammonia is a liquid, and could be easily adapted into the current liquid fuel infrastructure.³ Another benefit of ammonia over other hydrogen storage methods is that ammonia decomposition does not produce carbon monoxide, a common side product that is produced when carbon-based

compounds are used to produce hydrogen, which poisons fuel cell electrodes. The current best catalyst to decompose ammonia is single metal Ruthenium. However Ruthenium is very rare and would become very expensive if this process is adopted commercially. Thus, ammonia decomposition could make hydrogen a viable alternative energy source, if a cheaper catalyst could be found.

If ammonia can be found to be an economical energy carrier, that would be a big step towards a feasible hydrogen economy. Solar hydrogen, produced using carbon neutral water splitting, can be reacted with nitrogen from the air to form ammonia. This process is the most studied of any process using heterogeneous catalysis, and ammonia is the most produced industrial chemical on earth. Ammonia is used mainly as fertilizer, but by utilizing solar hydrogen the total production of ammonia could be increased to be used as an energy carrier as well. By pressurizing ammonia, it can be condensed into a liquid and used in the current infrastructure as a replacement for gasoline. Automobiles that are designed to run on ammonia would decompose ammonia onboard to produce hydrogen to meet the demands of the fuel cell. The only byproducts that would be produced by the vehicle would be nitrogen from the decomposition of ammonia and water from the fuel cell. Both products would not affect the environment adversely.

The main rationalization for the feasibility of ammonia is that the volumetric and gravimetric energy density is on par with the energy density of gasoline.¹ Another important fact to note about using ammonia as an energy carrier is that it would not change the current paradigm of energy. Changing the way that people get their energy

is not only difficult, but also expensive. The newer line of electric cars has not really taken off because people are used to getting their energy in a certain way. They aren't ready to spend money to get power ports installed in their homes, when they are not even sure if it will be a lasting technology. However, the beauty of ammonia technology is that it could be integrated into the current infrastructure, and while people would need to buy fuel cell cars, the refueling process would be the same as the current gasoline technology.

Ammonia synthesis is a reaction that has been well studied and is fully understood.⁴ There is significant work required to completely understand ammonia decomposition. Ruthenium is the most active single metal catalyst for the reaction, but , ruthenium is very expensive and scarce.⁵⁻⁸ If every automobile were to use ammonia as an energy carrier, there would not be enough ruthenium in the world to catalyze the decomposition. The main technical hurdle for using ammonia as an energy carrier is finding a more abundant and cheaper catalyst for ammonia decomposition. In order to lower costs and increase activity, bimetallic catalysts are potentially useful and will be examined for this reaction.

The work of Hansgen et al. found the ideal catalysts for ammonia decomposition through computational studies and surface science experiments. Microkinetic modeling was performed to determine the optimal nitrogen binding energy for a catalyst for ammonia decomposition, which was found to be 134kcal/mol.⁹ Using this information, screening was performed using density functional theory (DFT) to determine possible metal pairs that had this optimal

nitrogen binding energy. When two metals are combined to form a catalyst, it has been shown that one metal segregates to the surface, instead of forming a mixed alloy, to minimize the surface energy of the two-metal system.¹⁰⁻¹⁵ The NiPt family was found to show favorable results for ammonia decomposition. NiPt can form monolayer bimetallic surfaces such as Ni-Pt-Pt(111), and Pt-Ni-Pt(111).¹⁶ Temperature programmed desorption (TPD) was used to verify activity, and experiments determined that the active conformation of NiPt family is Ni-Pt-Pt(111). However, these descriptors have limitations. Assumptions must be made and uncertainty is present within the models, the source of which is the energetic predicted by DFT.¹⁷ Therefore, reactor experiments under pressure with supported catalysts will always be necessary to validate predictions made by computations or surface science experiments.

Bimetallic surfaces exhibit properties that are different from bulk bimetallic alloys, and by combining two metals the electronic and chemical properties of the resulting catalyst will be different than the two parent metals.¹⁸⁻²⁰ One of the first methods for trying to predict the properties of a bimetallic catalyst is to use the periodic table to interpolate an important descriptive parameter, such as binding energy, in an effort to increase activity.²¹ Before more sophisticated methods for determining binding energies, such as DFT, were developed interpolation was used to approximate these bimetallic binding energies. However, interpolation of binding energies can fail for monolayer bimetallic systems. The nitrogen binding energies of monolayer Ni-Pt-Pt(111) and Pt-Ni-Pt(111) both fall outside of the binding energies of

Ni and Pt, so more accurate calculations are necessary. More sophisticated techniques, such as surface science experiments, and DFT calculations have also been applied to obtain more accurate measurements of binding energies. The screening of various catalysts can be performed by building metal lattices and calculating the change in energy when a species is adsorbed. Once catalysts are screened using DFT calculations, surface science experiments are performed, such as TPD to determine if the metal is an active catalyst.²² Pt has been shown to form a monolayer bimetallic when paired with a 3d metal, such as Ni.²³ In a reducing environment, the subsurface configuration of Pt-Ni-Pt(111) is thermodynamically preferred, and the surface configuration of Ni-Pt-Pt(111) is most stable in an oxidizing environment. The bimetallic configuration is important because the configuration affects the adsorbate binding energies, and therefore the activity.²⁴ Different adsorbates can alter the thermodynamics of the monolayer bimetallic catalyst, causing surface segregation. This is of critical importance to insuring the proper conformation is present.²⁵

The major difficulty in harnessing the NiPt catalyst is the large amount of hydrogen present on the surface, during the ammonia decomposition reaction, thermodynamically favors Pt to diffuse to the surface. However, in order to achieve the increased activity from the synergistic bimetallic effect, Ni must be on the surface. The true challenge will be ensuring that there is enough nitrogen adsorbed on the surface to provide the necessary oxidizing conditions to pull the Ni to the surface. At the higher temperatures required for activity we would expect the Ni to diffuse below the surface. However, the adsorbed nitrogen can stabilize the Ni on the surface.²⁶ An

affordable catalyst for ammonia decomposition would allow ammonia to become the future hydrogen carrier.

Chapter 2

METHODS

Microkinetic Modeling

Modeling of the reaction mechanism was done by assuming a 6 step mechanism for the reaction.

Table 2.1 List of Reactions in Ammonia Decomposition Mechanism

Ammonia Adsorption	$\text{NH}_3 + * \leftrightarrow \text{NH}_3^*$
1 st Hydrogen Cleavage	$\text{NH}_3^* + * \leftrightarrow \text{NH}_2^* + \text{H}^*$
2 nd Hydrogen Cleavage	$\text{NH}_2^* + * \leftrightarrow \text{NH}^* + \text{H}^*$
3 rd Hydrogen Cleavage	$\text{NH}^* + * \leftrightarrow \text{N}^* + \text{H}^*$
Nitrogen Desorption	$2\text{N}^* \leftrightarrow \text{N}_2 + 2^*$
Hydrogen Desorption	$2\text{H}^* \leftrightarrow \text{H}_2 + 2^*$

Within the model, each of the reactions were considered to be reversible and the forward and reverse reactions were considered separately such that each had their own pre-exponential factor and activation energy, adjusted for coverage. The parameters of the modeled reactor were taken to be as close to the reactor used in the brick and mortar lab, unless otherwise stated in an effort to compare the flow and batch systems. A significant difference between the batch and flow reactor is the surface area to volume ratio of the two systems. Due to less catalyst and much more volume being present in the batch reactor there is a difference of 5 orders of magnitude of the surface area to volume ratio between the two reactors and this trait

was accounted for in our models. For the flow reactor the surface area ratio was 9500 cm^{-1} , and for the batch reactor the surface area ratio was 0.43 cm^{-1} .

Synthesis

Incipient wetness impregnation was used to synthesize various NiPt bimetallic catalysts by varying metal loading and impregnation sequence. $\gamma\text{-Al}_2\text{O}_3$ was used as the support for all of the catalysts synthesized. The Ni and Pt precursor solutions were made by adding distilled water to the prescribed amount of metal salt. The metal salts utilized were $\text{Pt}(\text{NH}_3)_4(\text{NO}_3)_2$ and $\text{Ni}(\text{NO}_3)_2 \cdot 6\text{H}_2\text{O}$. Both were purchased from Alfa Aesar. Three monometallic catalysts were also synthesized as controls. The synthesis procedure for drying the catalyst was 10 hours at 373K, followed by calcination for 2 hours at 563K. For the bimetallic catalysts that were impregnated separately, the drying procedure was repeated for each metal loading.²⁷

CO Pulse Chemisorption

CO pulse chemisorption experiments provided a means to characterize the surface area of each catalyst (normalized per gram catalyst). This is accomplished by measuring the CO uptake of the catalyst, which is proportional to the surface area. To determine the CO uptake an AMI-200ip (Altamira Instruments) was used. About 100mg of catalyst was loaded into a quartz U-tube, packed on both sides by quartz wool. The catalyst was reduced in a 1:1 hydrogen/helium mixture for 1 hour at 723K. After purging and cooling in He, CO pulses of 20 sccm were used with a He carrier gas. A thermal conductivity detector (TCD) was used to measure the amount of CO

that passes through the catalyst. The amount of CO adsorbed was calculated by subtracting the amount of CO that was observed by the TCD from the original amount of CO contained in each pulse.

Extended X-ray absorption fine structure (EXAFS)

EXAFS measurements were used to identify the presence of bimetallic bonds and measure the extent of bimetallic formation in the catalyst particles. EXAFS can also be used to determine the number of nearest neighbors, nearest neighbor atom type, and distance to neighbors. This information can give a better idea to the size and shape of the nanostructures on the surface of the support.²⁸⁻²⁹ By measuring the Pt L_{III} edge we can determine the presence of Pt-Ni bonds. EXAFS experiments were performed at Brookhaven National Laboratory, using beamline X18B and X19A of the National Synchrotron Light Source (NSLS). The mass of catalyst used was calculated so that the thickness of a pellet would be two adsorption lengths. This yields to the best quality of data and reduction of noise. The catalyst was pressed into a pellet using a force of about 3 tons. The pellets were then loaded on a custom-made sample holder that secures the pellet while it sits in an in situ reduction cell. The samples were reduced in 5% H₂/He and heated to 723K at a rate of 10K/min using a thermal cartridge. The pellets soaked for 1 hour and then were allowed cool to room temperature still in the hydrogen environment. After scans of the reduced catalyst were taken at room temperature, 5% NH₃/He was dosed into the cell. The same heating procedure was then utilized to simulate reaction conditions, and the pellet was

allowed to soak in ammonia at 723K for 2 hours while scans were taken. A double crystal Si(111) monochromator was used to take scans. Both the incident and transmitted signals were detected using ionization chambers. A Pt foil was utilized to calibrate the EXAFS energy scans to the Pt L-III edge. The data were fit using Athena software. Artemis is then used to fit the data in order to calculate coordination numbers and distances.

EXAFS measurements for each scan were collected in three regions. All of the energies reported are based on the Pt L3 edge of 11563 eV. The pre-edge region from -150eV to -25eV was examined using a step size of 5eV and an integration time of 1s. The edge region beginning at -25eV to 40eV used a smaller step size of 0.5eV and a longer integration time of 2s. The post-edge region ranged from the 40eV to 18k (which is about 1450eV) after the edge, using a step size of 0.05k and a 2s integration time.

The EXAFS scans themselves were analyzed using IFFEFIT.³⁰⁻³² The scans were aligned to a reference foil, and deglitching was done. Multiple scans were merged together in an effort to reduce the contribution due to experimental noise. Once the data was merged the scans were transformed into R-space so that data fitting could be accomplished. Only the first shells of the fittings were fit. Pt-Pt fittings were accomplished by using the Pt fcc structure found in Atoms. The Pt-Ni bonds were fit by taking that same Pt fcc structure and changing the coordination environment such that all of the atoms nearest to the object Pt atom were assumed to have the properties of a Ni atom.

Flow Reactor Studies

Reactor studies are used to measure the activity of each catalyst. A ¼ in. quartz reactor was used to house the catalyst and perform the reaction. NH₃, H₂, N₂, and He were all fed to the reactor using stainless steel tubes and MKS mass flow controllers to control the gas flow rates. For each run 100mg of catalyst was used and diluted with 150 mg of inert Al₂O₃, with particle size 50-75 µm. The catalyst was diluted to reduce temperature and concentration gradients. This decreases the mass transfer limitations of the catalyst.³³ After the catalyst mixture was packed into the reactor, the resulting bed length was about 1 inch. A gas phase thermocouple located on the downstream side of the catalyst was used to control the reaction temperature. Before any reactor studies were performed, the catalyst was reduced in 200 sccm of 10% H₂ in He for 2 hours at 450°C with a ramp rate of 10°C/min. A HP Series 5890 gas chromatograph (GC) with a thermal conductivity detector was used to measure the concentration of the outlet stream. The conversion was calculated using the NH₃ and N₂ peaks.³⁴

FTIR Batch studies

The design of the batch reactor was based a design in the literature.³⁵⁻³⁶ Fourier transform infrared spectroscopy was used to measure the gas-phase concentrations of ammonia in the batch reactor. The instrument allows for in situ reduction and reaction of samples while taking spectroscopic measurements of gas-

phase species. Using a Thermo Nicolet Nexus 470 spectrometer equipped with a MCT-A (mercury cadmium telluride) detector, spectra were taken with 4cm^{-1} resolution.

Chapter 3

RESULTS

Microkinetic Modeling

Modeling was employed to explain the differences between the batch reactor and flow reactor. In order to effectively use the results from the modeling we first modeled the reactors using the parameters to simulate the lab-scale batch and flow reactor using a nitrogen binding energy of 130kcal/mol. This important descriptor should accurately simulate the NiPt catalyst in the surface Ni configuration.

Flow Reactor

The flow reactor was modeled assuming a catalyst bed of 2.54cm, and an internal diameter of 4mm. The total flow rate of the reactor was 200 sccm, 10% ammonia, diluted with argon. This results in a residence time of 0.1s. The pressure throughout the reactor was assumed to be 1 atm and various temperatures were studied. The conversions calculated in our differential flow reactor are compared to the equilibrium conversion we would expect from an infinitely long reactor.

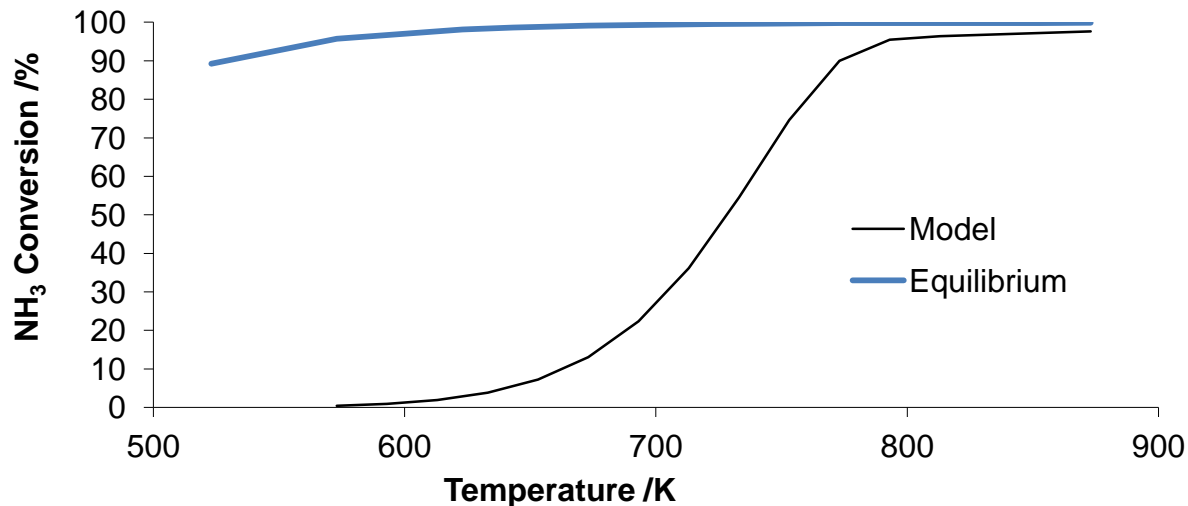


Figure 3.1 Ammonia Conversion Predicted by Model at Laboratory Conditions Compared to Thermodynamic Equilibrium

At lower temperatures, the reactor is in the kinetic regime, as the temperature increases the reaction is equilibrium controlled. It is important to note that although the equilibrium conversion for this reaction is high, there is still a significant kinetic barrier to overcome. Reaction is only observed at relatively high temperatures as compared to hydrogenation or reforming chemistries that have been previously shown to be active with this catalyst.^{16,27,37-39}

Batch Reactor

The batch reactor is run at sub-atmospheric pressures. Experimentally, this is done so that the gas phase concentration can be measured using IR-spectroscopy. Due to the lower pressures present in the reactor pure ammonia can be fed into the batch reactor. The following simulation was performed at 723K and 0.02 atm. For both the

model and the experiments a constant volume reactor is used. Again the optimal nitrogen binding energy of 130 kcal/mol is used as the main descriptor of the surface Ni configuration NiPt catalyst.

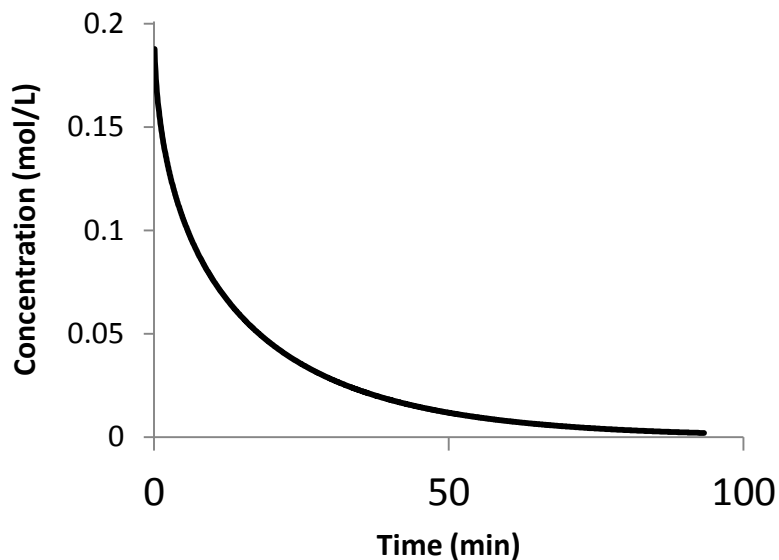


Figure 3.2 Model Predicted Ammonia Concentration as a Function of Time

Due to the small area to volume ratio, compared to the flow reactor, long time scales are needed, in order to consume all of the ammonia. While the nature of the batch reactor is obviously not steady-state, the surface coverages of hydrogen and nitrogen on the catalyst reach equilibrium quickly.

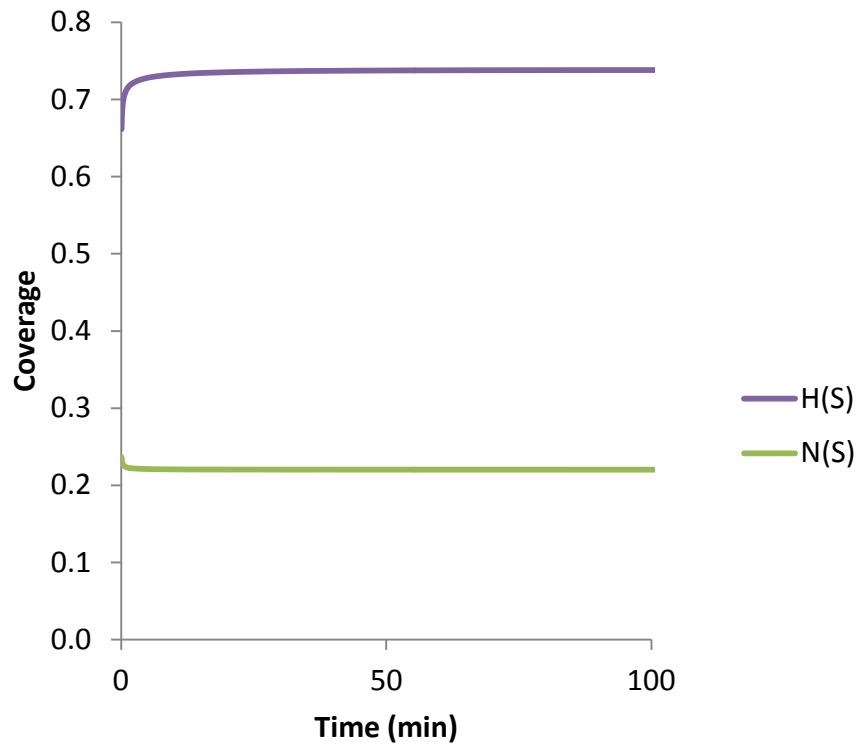


Figure 3.3 Coverages of Nitrogen and Hydrogen Found by Model in Batch Reactor

It is important to be able to compare the coverages of the two reactors under equal conditions to understand more about the stability of the catalyst. The following plot shows the coverages of both reactor systems under the conditions of 1 atm, 723K, 10% ammonia. The plot uses contact times that make physical sense for the flow reactor, and short times in the batch.

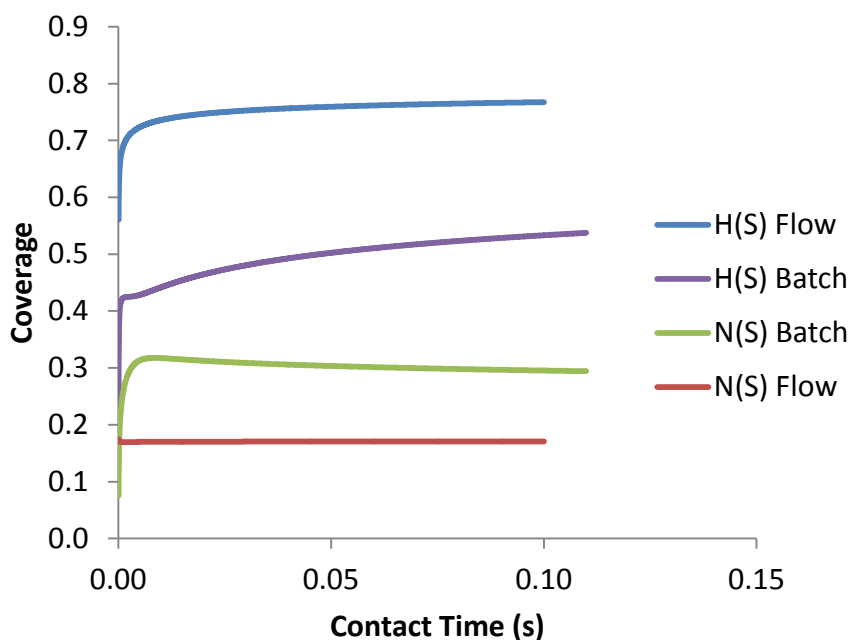


Figure 3.4 Comparing the Coverages at Low Contact Times for Both Systems

The first point to notice about the coverages in the different reactor systems are that the flow reactor coverages match those of the batch reactor at long times. Also, examining the coverage for the batch reactor at short times gives us an insight into how the coverages vary during the initial stages of the reaction as compared to pseudo steady-state surface concentrations. At short times the nitrogen concentration is higher and the hydrogen concentration is lower than the equilibrium coverages. When higher nitrogen coverages and lower hydrogen coverages are present the surface Ni configuration of the bimetallic is more stable.²⁵ The key to unlocking the synergistic activity of the bimetallic catalyst as predicted from surface science may rely on harnessing these low contact time batch surface concentrations.

Steady-State Flow Reactor

The following data was taken at 723K. After the catalyst was reduced in situ, 200 sccm of 10% ammonia (diluted with He) was fed to the reactor. The plot shows turnover frequency as a function of time on stream. Turnover frequency was calculated by measuring the moles of ammonia that react and comparing them to the moles of active sites. CO pulse chemisorption was used to determine the moles of active sites of the catalyst, assuming a stoichiometry of 1:1, which is assumed to be an accurate measure of surface area.

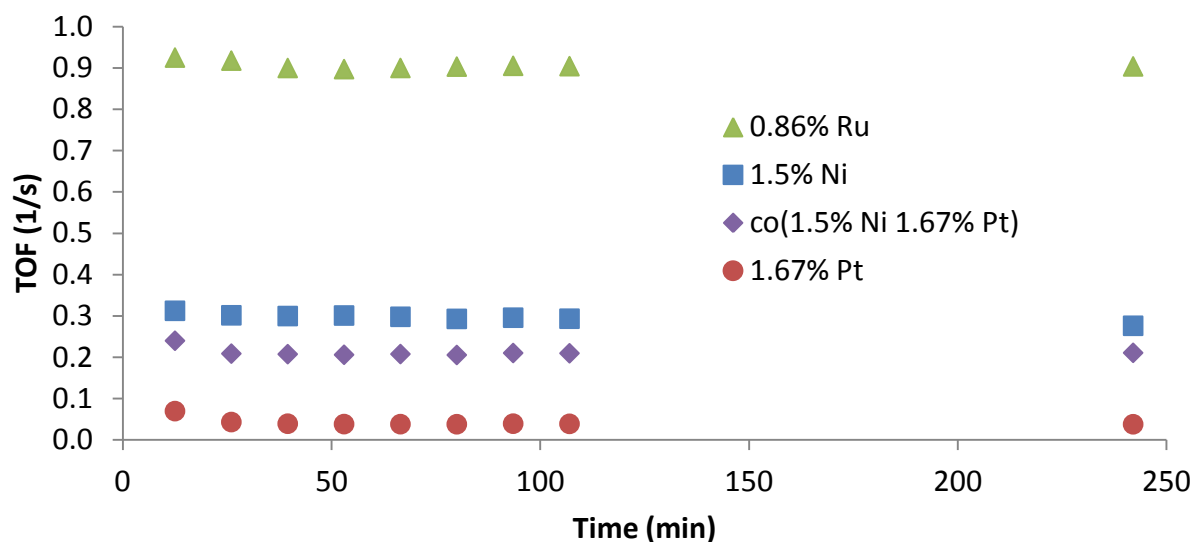


Figure 3.5 Steady-State Turnover Frequencies Comparing Different Metal Catalysts

The steady state flow reactor data shows that the monometallic catalyst actually outperforms the bimetallic catalyst, when the catalysts are normalized based on surface area. This is an indication that the active surface Ni configuration is not

present in the flow reactor. This data speaks to the importance of the stability of the catalyst. While we can use modeling and surface science to predict the activity of a supported catalyst, it is still difficult to predict the nanoparticle structure of the catalyst support. For the ammonia decomposition the stability and structure of the catalyst is critical for activity to be observed.

Batch Reactor

The batch FTIR data was fit using the data between 5 and 40 minutes, assuming a first order rate constant. The following table lists the rate constants tabulated from the data and normalizes the rate based on the total number of surface sites. The data from the batch reactor shows that the bimetallic catalyst outperformed the monometallic catalyst on a mass basis. However, also like the flow reactor, on a surface area basis the monometallic Ni outperforms the bimetallic catalyst.

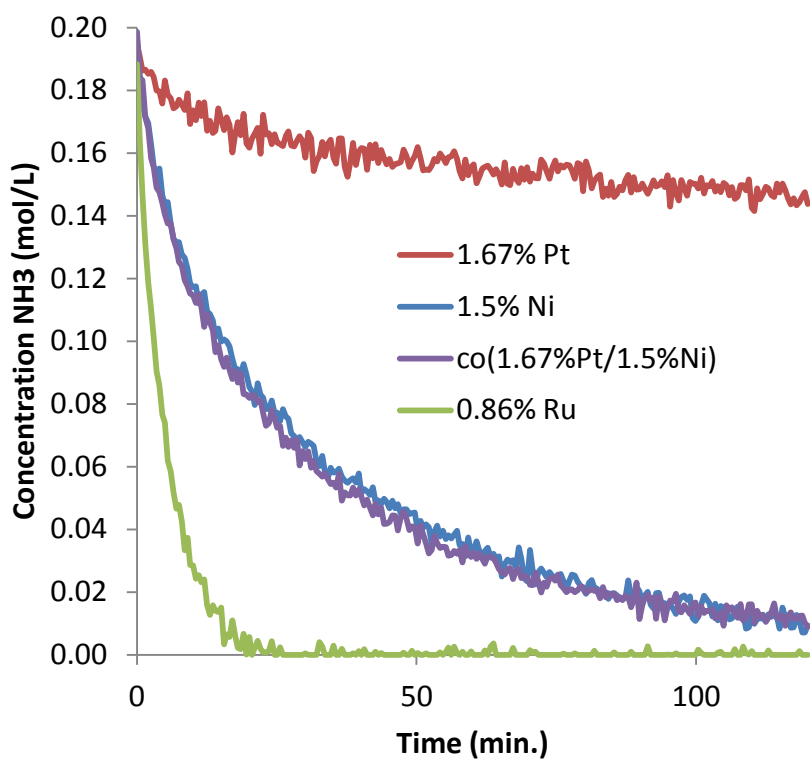


Figure 3.6 Comparing Ammonia Concentration as a Function of Time Across Different Metal Catalysts

Table 3.2 Summary Table of Rate Constants of Different Metal Catalysts

	k (min⁻¹)	mass (g)	k(min⁻¹g⁻¹)	Area(μmol/g)	k(min⁻¹ mmol⁻¹ catalyst)
NiPt	2.93E-02	0.0248	1.18E+00	50.2	23.5
Ni	2.79E-02	0.0253	1.10E+00	28.8	38.3
Ru	2.19E-01	0.0256	8.55E+00	59.2	144.5
Pt	3.17E-03	0.0256	1.24E-01	34.8	3.6

From the batch reactor data, we can make conclusions similar to those drawn from the flow reactor. The bimetallic catalyst does not yield a significant boost in activity on the site basis or mass basis. This is due to the fact that at these higher

temperatures there is not enough adsorbed nitrogen bound to the surface to stabilize the Ni at the surface.

EXAFS

The table lists the coordination environment for the catalyst at 723K for the hydrogen treatment and the ammonia treatment. From the data we can include that within the standard error the coordination structure of the catalyst does not change whether the catalyst is exposed to hydrogen or ammonia. Therefore we can infer that the catalyst is Pt-terminated in the presence of ammonia.

Table 3.3 Summary Chart of EXAFS Results (Coordination Number, Bond Distance, Bond Type) Comparing the Catalyst in a Reducing Environment to the Same Catalyst in Ammonia

Treatment	Pt-Pt		Pt-Ni		Sigma squ.
	Coord #	Bond Length (A)	Coord #	Bond Length (A)	
Hydrogen @ 723K	4.5±2.4	2.668±0.044	3.7±1.5	2.555±0.024	0.013±0.003
Ammonia @ 723K	5.3±0.8	2.691±0.014	3.9±0.5	2.579±0.008	0.013±0.001

When we compare the catalyst in hydrogen to the catalyst in the ammonia reaction environment, we observe no discernable difference in the coordination environment. This again speaks to the issue of stability. The hope was that the adsorbed nitrogen from the ammonia would bind to the catalyst and help to stabilize the Ni on the surface. Using the EXAFS fittings, we can now infer that the reason that the bimetallic catalyst is not active is that the Ni-terminated bimetallic nanoparticle is not present in our supported catalyst. This is the cause of the disconnect between the reactor experiments and the surface science work done previously in the group.⁹

Chapter 4

DISCUSSION

This work assumes that the surface Ni configuration of the NiPt catalyst would be active for the ammonia decomposition reaction. However a second interpretation of the initial surface science experiments leads to some interesting observations. Looking initially at the work of Hansgen et al.⁹, the TPD peaks in fact appear to be first order due to their asymmetric shape. This is an unexpected result due to the fact that in order for nitrogen to desorb, two nitrogen atoms must come together to enter into the gas phase. Theoretically, a nitrogen TPD should show second order behavior.

One possible explanation for the first order behavior is that the reaction occurs as a result of surface rearrangement. When that information is coupled to the fact that the desorption peaks begins at the temperature where the Ni diffuses into the surface. This is known from the synthesis conditions given in the work⁹, and it is also studied in more detail in the work of Menning et al.²⁴ The same trend can be observed in another work of Hansgen et al.⁴⁰, where we see the TPD peaks of other Pt-3d bimetallics starting to occur where we know that the 3d metal would diffuse into the surface, thus creating the weaker and less active bimetallic surface.

Bringing together all of this new interpretation of the surface science experiments, different conclusions can be drawn. It is possible that the binding energies of all of these bimetallic surfaces were undercalculated. This would result in the phenomenon observed in the TPD experiments. As thought, the Ni-Pt-Pt surface is present at the lower temperatures at the beginning of the TPD experiments. However,

this surface as such a high binding energy, that while the ammonia decomposes on the surface, the nitrogen and hydrogen do not desorb. Desorption is only observed once the catalyst is heated past a certain point (for NiPt 600K). At this point the Ni is no longer stable on the surface and diffuses underneath the now Pt surface. While the Pt-Ni-Pt surface is not active for the ammonia decomposition reaction, it is an excellent surface for the already decomposed nitrogen and hydrogen to now easily desorb into the gas phase. This is a much more likely explanation of the surface science ammonia TPDs that were the experiments that led to this work.

Using this interpretation of the results would lead to a different methodology for determining an ammonia decomposition catalyst. For a supported NiPt catalyst to work, it would need to cycle between the surface Ni and surface Pt configurations in order to perform the reaction and then allow the surface products to desorb. In order to do this at measurable rates either the chemical environment of the reactor or temperature of the reactor would need to be cycled so that each configuration would in turn be dominant. A reactor design that utilized these principles would not be economically feasible at ambient temperatures. The surface science experiments were only able to show promise due to the small number of molecules that were reacting at one time. An optimal catalyst for this reaction will not cycle between desorption-limited or reaction-limited, but its binding energy will be balanced and optimized between these two steps that are necessary for reaction to occur continuously.

Chapter 5

CONCLUSIONS

Supported NiPt catalysts were synthesized and models were prepared to validate the activity of a catalyst that was predicted to be active using a multiscale approach. This NiPt catalyst was explored previously using UHV temperature programmed desorption experiments, and its activity measured. Experiments were performed in both batch and flow configurations, and models were prepared to predict the conversion that would be observed if the activity predicted by the UHV system bridged the gap to the supported catalyst. EXAFS characterization was performed to determine if the coordination environment changed in the presence of ammonia, compared to the coordination environment of the catalyst reduced in hydrogen.

From our models of the optimal surface Ni configuration catalyst and the experiments that compare the activities of the bimetallic NiPt catalyst to the analogous monometallic catalyst, the surface Ni configuration is not present in the ammonia environment in either of the two reactor systems. The NiPt-ammonia system is an example of a chemistry that does not directly correspond to surface science experiments due to the poor stability of the catalyst. It has been shown that at temperatures above 600K Ni prefers to diffuse into the subsurface layer as Pt segregates to the surface.^{22,26} It had been hypothesized that the nitrogen adsorbed to the surface of the catalyst would help to stabilize the catalyst and keep the Ni from

diffusing into the bulk of the catalyst. However, the amount of nitrogen present was not enough to offset the reducing effect of the surface hydrogen also present on the surface of the catalyst. At the temperatures required for ammonia decomposition to occur in appreciable quantities, it is not possible to obtain the surface Ni configuration of the NiPt catalyst, which has been predicted previously by surface science experiments to show increased synergistic activity for the ammonia decomposition reaction. Thus explaining why the bimetallic catalyst synthesized in this study is not as active as the parent monometallic Ni catalyst.

REFERENCES

- (1) Züttel, A.; Remhof, A.; Borgschulte, A.; Friedrichs, O. *Philosophical Transactions of the Royal Society A: Mathematical, Physical and Engineering Sciences* **2010**, *368*, 3329.
- (2) Yin, S. F.; Xu, B. Q.; Zhou, X. P.; Au, C. T. *Applied Catalysis A: General* **2004**, *277*, 1.
- (3) Deshmukh, S. R.; Mhadeshwar, A. B.; Vlachos, D. G. *Industrial & Engineering Chemistry Research* **2004**, *43*, 2986.
- (4) Boisen, A.; Dahl, S.; Nørskov, J. K.; Christensen, C. H. *Journal of Catalysis* **2005**, *230*, 309.
- (5) Logadóttir, Á.; Nørskov, J. K. *Journal of Catalysis* **2003**, *220*, 273.
- (6) Ganley, J. C.; Thomas, F. S.; Seebauer, E. G.; Masel, R. I. *Catalysis Letters* **2004**, *96*, 117.
- (7) Choudhary, T. V.; Sivadinarayana, C.; Goodman, D. W. *Catalysis Letters* **2001**, *72*, 197.
- (8) Prasad, V.; Karim, A. M.; Ulissi, Z.; Zagrobelny, M.; Vlachos, D. G. *Chemical Engineering Science* **2010**, *65*, 240.
- (9) Hansgen, D. A.; Vlachos, D. G.; Chen, J. G. *Nat Chem* **2010**, *2*, 484.
- (10) Kitchin, J. R.; Reuter, K.; Scheffler, M. *Physical Review B* **2008**, *77*, 075437.
- (11) Campbell, C. T. *Annual Review of Physical Chemistry* **1990**, *41*, 775.
- (12) Tao, F.; Grass, M. E.; Zhang, Y.; Butcher, D. R.; Renzas, J. R.; Liu, Z.; Chung, J. Y.; Mun, B. S.; Salmeron, M.; Somorjai, G. A. *Science* **2008**, *322*, 932.
- (13) Ruban, A. V.; Skriver, H. L. *Computational Materials Science* **1999**, *15*, 119.

- (14) Ma, Y.; Balbuena, P. B. *Surface Science* **2008**, *602*, 107.
- (15) Pallassana, V.; Neurock, M.; Hansen, L. B.; Hammer, B.; Nørskov, J. K. *Physical Review B* **1999**, *60*, 6146.
- (16) Humbert, M. P.; Chen, J. G. *Journal of Catalysis* **2008**, *257*, 297.
- (17) Prasad, V.; Vlachos, D. G. *Industrial & Engineering Chemistry Research* **2008**, *47*, 6555.
- (18) Rodriguez, J. A. *Surface Science Reports* **1996**, *24*, 223.
- (19) Rodriguez, J. A.; Goodman, D. W. *Science* **1992**, *257*, 897.
- (20) Kitchin, J. R.; Nørskov, J. K.; Barteau, M. A.; Chen, J. G. *The Journal of Chemical Physics* **2004**, *120*, 10240.
- (21) Jacobsen, C. J. H.; Dahl, S.; Clausen, B. S.; Bahn, S.; Logadottir, A.; Nørskov, J. K. *Journal of the American Chemical Society* **2001**, *123*, 8404.
- (22) Kitchin, J. R.; Khan, N. A.; Barteau, M. A.; Chen, J. G.; Yakshinskiy, B.; Madey, T. E. *Surface Science* **2003**, *544*, 295.
- (23) Mun, B. S.; Watanabe, M.; Rossi, M.; Stamenkovic, V.; Markovic, N. M.; Ross, J. P. N. *The Journal of Chemical Physics* **2005**, *123*, 204717.
- (24) Menning, C. A.; Chen, J. G. *The Journal of Chemical Physics* **2008**, *128*, 164703.
- (25) Menning, C. A.; Chen, J. G. *The Journal of Chemical Physics* **2009**, *130*, 174709.
- (26) Wang, H.; Stamatakis, M.; Hansgen, D. A.; Caratzoulas, S.; Vlachos, D. G. *The Journal of Chemical Physics* **2010**, *133*, 224503.
- (27) Lonergan, W. W.; Vlachos, D. G.; Chen, J. G. *Journal of Catalysis* **2010**, *271*, 239.
- (28) Karim, A. M.; Prasad, V.; Mpourmpakis, G.; Lonergan, W. W.; Frenkel, A. I.; Chen, J. G.; Vlachos, D. G. *Journal of the American Chemical Society* **2009**, *131*, 12230.

- (29) Frenkel, A. I.; Hills, C. W.; Nuzzo, R. G. *The Journal of Physical Chemistry B* **2001**, *105*, 12689.
- (30) Newville, M. *Journal of Synchrotron Radiation* **2001**, *8*, 322.
- (31) Ravel, B.; Newville, M. *Journal of Synchrotron Radiation* **2005**, *12*, 537.
- (32) Rehr, J. J.; Albers, R. C. *Reviews of Modern Physics* **2000**, *72*, 621.
- (33) Prasad, V.; Karim, A. M.; Arya, A.; Vlachos, D. G. *Industrial & Engineering Chemistry Research* **2009**, *48*, 5255.
- (34) Chellappa, A. S.; Fischer, C. M.; Thomson, W. J. *Applied Catalysis A: General* **2002**, *227*, 231.
- (35) Barzetti, T.; Selli, E.; Moscotti, D.; Forni, L. *Journal of the Chemical Society, Faraday Transactions* **1996**, *92*, 1401.
- (36) Basu, P.; Ballinger, T. H.; J. T. Yates, J. *Review of Scientific Instruments* **1988**, *59*, 1321.
- (37) Lu, S.; Lonergan, W. W.; Bosco, J. P.; Wang, S.; Zhu, Y.; Xie, Y.; Chen, J. G. *Journal of Catalysis* **2008**, *259*, 260.
- (38) Humbert, M. P.; Murillo, L. E.; Chen, J. G. *ChemPhysChem* **2008**, *9*, 1262.
- (39) Bertolini, J.-C. *Applied Catalysis A: General* **2000**, *191*, 15.
- (40) Hansgen, D. A.; Thomanek, L. M.; Chen, J. G.; Vlachos, D. G. *The Journal of Chemical Physics* **2011**, *134*, 184701.